Journal of Marine Science and Technology

Volume 23 | Issue 6 Article 2

SEABED SCOUR AROUND A BREAKWATER A CASE STUDY IN MAILIAO HARBOR

I-Fu Lin
Department of Marine Environment and Engineering, National Sun Yat-sen University, Kaohsiung, Taiwan. R.O.C

I-Fan Tseng
Department of Marine Environment and Engineering, National Sun Yat-sen University, Kaohsiung, Taiwan. R.O.C, ifan@mail.nsysu.edu.tw

Chung-Pan Lee
Department of Marine Environment and Engineering, National Sun Yat-sen University, Kaohsiung, Taiwan. R.O.C

Guan-Yu Chen
Department of Oceanography, National Sun Yat-sen University, Kaohsiung, Taiwan. R.O.C.

SEABED SCOUR AROUND A BREAKWATER A CASE STUDY IN MAILIAO HARBOR

Acknowledgements

This study was supported by the Harbor and Marine Technology Center, Institute of Transportation, Ministry of Transportation and Communications, R.O.C., Project No. MOTCIOT-103-H2DB005d.

Journal of Marine Science and Technology, Vol. 23, No. 6, pp. 846-854 (2015)
DOI: 10.6119/JMST-015-0610-1

SEABED SCOUR AROUND A BREAKWATER A CASE STUDY IN MAILIAO HARBOR

I-Fu Lin[1], I-Fan Tseng[1], Chung-Pan Lee[1], and Guan-Yu Chen[2]

Key words: erosion, excess shear stress, scour potential model.

ABSTRACT

According to a field measurement in 2012, the bathymetry in the area of Mailiao Harbor, located in the middle of Taiwan's west coast, has scouring hole with a size distribution of approximately 500 × 100 m. The maximum scour depth is 26 m (from −22 m eroded to −48 m). Although scour has become a major threat to breakwaters and navigational safety, it can be predicted cost-effectively, reliably, and rapidly by applying the computational fluid dynamics (CFD) numerical simulation. In this study, numerical simulation of tidal current and typhoon waves was performed to investigate the causes of the scouring hole in the Mailiao Harbor sea area. Current field data from an acoustic Doppler current profiler (ADCP) were used as the requirements of tidal boundaries. A fixed-bed bottom boundary was generated using sounding data from the year 1996, and the harbor computer-aided design (CAD) physical model was used as the requirement of the closing boundary. Moreover, the sensitivity of grid independence and numerical domain was tested to create a steady flow field. The study results indicated that a vorticity form at the lee side of the breakwater during tidal cycles conformed to tidal current data with numerical modeling. Furthermore, describe the distribution of fluid velocity, excess shear stress and tidal current by visualization, the application of scour potential model with the Stokes 5th order wave boundary is found to give more reasonable results.

I. INTRODUCTION

Wave or tidal current may scour the bottom of submarine structures, damaging or even toppling the structures. For example, in a submarine relief near a harbor breakwater head, the concentration, underwashing, or turning of waves and tidal currents may scour the breakwater head. This study focused on Mailiao Harbor, located in the middle of Taiwan's west coast, as an example, In the harbor, the original design depth at the west breakwater head was approximately −22 m. According to submarine relief measurements in 2012, a chasm of approximately 500 × 100 m formed on the sea bed near the breakwater head in Mailiao Harbor, the inmost depth of the chasm is −48 m and the erosion depth has reached 26 m. This chasm endangers the breakwater body and ships in the harbor. A reliable and economical mechanism for rapidly forecasting submarine relief erosion of the breakwater head can be provided using CFD numerical simulation.

In this study, the FLOW-3D CFD software was used to numerically simulate the wave and tidal current fields of this sea area. The observed real-time tidal level and typhoon waves over a 50-year return period in the open sea of Mailiao Harbor were used as open water boundary conditions, and the fixed-bed bottom boundary was established according to the observed depth. The physical model of the harbor was a closed boundary, and flow-field stability was calculated according to grid independence and the results of computational domain boundary sensitivity tests. The sequential water level, flow direction, and flow velocity of tidal currents in the simulation results were consistent with those recorded in the onsite observation data. The breakwater head formed a periodic eddy current with floods and ebbs. The relationship of the distribution of excess shear stress and the vortex effect at the bottom of the eddy zone to the bottom scour was visualized. The results were obtained using the Stokes fifth-order wave generation boundary and the renormalization group (RNG) turbulence model.

II. RESEARCH SCOPE

Mailiao Harbor in the Yunlin Offshore Industrial Park is located at the southern mouth of the Zhuoshui River. Since the harbor's construction in 1994, its north breakwater has been recharged by river sediment, as shown in Fig. 1. West breakwater III construction began in March 1998 and continued until September 2000.

Because of the extension of breakwater, tidal effects, and sand loads from the northern Zhuoshui River, the morphology of the erosion and deposition conditions at the toe of the

Paper submitted 12/17/14; revised 01/29/15; accepted 06/10/15. Author for correspondence: I-Fan Tseng (e-mail: ifan@mail.nsysu.edu.tw).
[1] Department of Marine Environment and Engineering, National Sun Yat-sen University, Kaohsiung, Taiwan. R.O.C.
[2] Department of Oceanography, National Sun Yat-sen University, Kaohsiung, Taiwan. R.O.C.

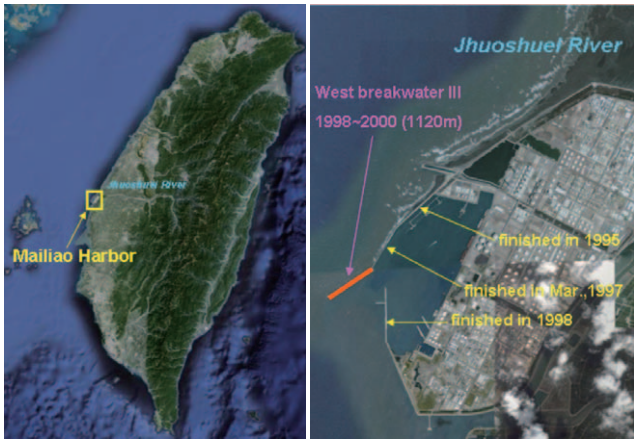

Fig. 1. Research scope: Mailiao Harbor.

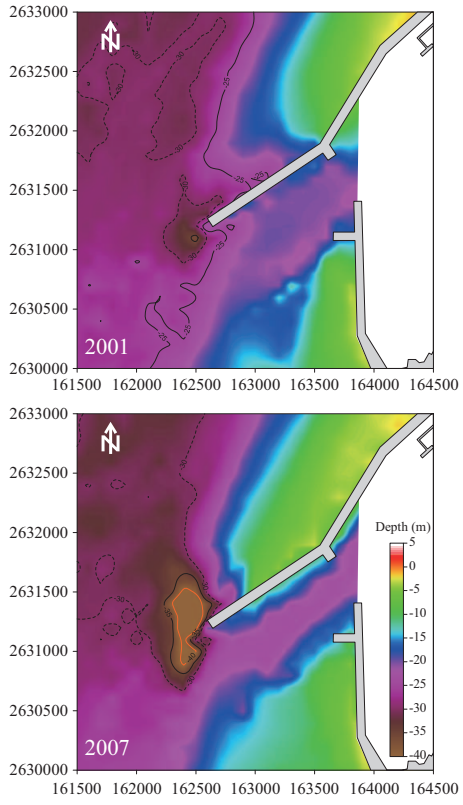

Fig. 2. Seafloor topography of Mailiao Harbor (2001, 2007).

western breakwater of Mailiao Harbor had dramatically changed. The water depth of the western breakwater in Mailiao Harbor in 2000 was approximately 22 m; approximately 500 × 300 m of the scour hole at the western side of the pier head was formed in 2001. The cross-sectional area and volume of erosion increased yearly, and the erosion reached the maximum in 2007, as shown in Fig. 2. However, the cross-sectional area and volume of erosion decreased each year after 2007, and the scour hole recovered slightly between 2007 and 2011.

III. LITERATURE REVIEW

The breakwater structure fluid-solid interaction and hydro-dynamic model applied to the wave and tidal field calculation are discussed as follows.

1. Scour Around Breakwater

General breakwater: In researching the relationship between the Port Kashima breakwater toe structure degradation and waves, Sato and Irie (1970) found that the further the wave deviated from the normal incident angle, the larger was the topographical change.

Vertical-wall breakwater: Researchers (Sumer and Fredsøe, 1997; Sumer and Fredsøe, 2000; Sumer et al., 2001; Sumer et al., 2005; Myrhaug and Ong, 2009) conducted experimental investigations regarding the characteristics and mechanism of topographical erosion near the vertical-wall breakwater head. These investigations were performed at sites with and without breakwater head foundation protection and wave current interaction. However, although these researchers did not investigate deep water areas, their results were references for this study. The aforesaid research findings are summarized as follows:

(1) Effect of wave-induced current on breakwater head erosion: When the wave incidence direction is normal to the breakwater body, the vortex formed at the breakwater side is the dominant mechanism for erosion. The relationship between the wave characteristics and levee body size can be expressed as a Keulegan-Carpenter (KC) parameter (= U_mT/B). When KC < 1, no obvious vortex flow occurs in the flow field; when 1 < KC < 12, the flow field forms a wake vortex behind the breakwater; when KC > 12, in addition to the wake vortex behind the breakwater, a horseshoe vortex occurs in front of the breakwater. If the wave-induced current acts simultaneously (in the same direction), then the scour depth is correlated with the wave-induced current divided by the bottom flow velocity initiated by the wave. When the Shields parameter exceeds the threshold, the relative scour depth of the bottom (ratio of scour depth to dike width) increases with the KC number; when only the wave-induced current velocity is effective, the scour depth increases (Sumer and Fredsøe, 1997; Sumer et al., 2005).

(2) Wave action on breakwater head erosion with foundation protection: When the wave incidence direction is normal to the breakwater body, the scour is severe; when the bottom flow initiated by waves is parallel with the breakwater, a scour channel may form along the breakwater toe. The amplitude of the scour can be reduced if foundation protection works for the bottom are present; a wider foundation protection layer offers more protection. When no foundation protection facility is present at the breakwater head, the ratio of the foundation protection width to the levee body width is Lp/D = 0, and the scour depth increases substantially. When the ratio of the foundation protection width to the levee body width is Lp/D > 3.6, the scour depth amplitude at the breakwater head can be

suppressed. Similar results were verified in the case of irregular waves (Sato and Irie, 1970; Gokce et al., 1994; Myrhaug et al., 2004; Myrhaug and Ong, 2009).

(3) Breakwater head erosion of wave action on upright breakwater and slope-dumped rock embankment: Wave steepness, water depth in front of a breakwater, and breakwater slope crucially influence scour because the slope-dumped rock embankment reduces the amplitude of erosion in front of a breakwater more than an upright breakwater does (Sumer et al., 2001).

2. Applying the Hydrodynamic Model to Calculate Wave and Current-Field

Dentale and Carratelli (2012) built the breakwater protection model according to the configuration of hydraulic model testing, to simulate the three-dimensional (3D) rubble slope bottom analyze the reflection, transmission, run-up, overtopping, and surf of wave current on the wave trap, as well as the stability of the structural foundation. Lai (2009) used this model to calculate the wave transformation, flow-field, and turbulence characteristics of an impervious and porous bed. The results showed that direct three-dimensional simulations can resolve the wave and velocity profile more complete and reasonable descriptions from outer to the inner porous layer and it is true no matter in the surf zone, swash zone and within the porous layer. Because of the friction and infiltration of porous layers, wave energy dissipates between the surf and swash zones, and flow-field and turbulence characteristics are distinct. Achartya (2011) used the turbulence model of FLOW-3D to simulate a series of spur-dike-plane bottom-scour mechanisms, and quantitatively analyzed longitudinal, lateral, and vertical plane turbulent flow fields around the spur dike. A spatial variation in wave height and water level is found between the submerged breakwater and the vertical seawall, and the maximum wave height occurs at the location of the antinodes. The spatial variation of water set up behind the submerged breakwater is similar to that of the wave height (Hirt and Sicilian, 1985).

IV. THEORETICAL BASIS

In this study, simulations of 3D flow through the scour around the breakwater were performed using FLOW-3D V10.1. This software includes a CFD code that can be used to solve fully 3D transient Navier-Stokes equations by using a finite-volume finite-difference method in a fixed Eulerian grid. This code was chosen for this study because of its flexibility and functionality in the scour potential model. The method used in the present study has been described in detail by Hirt (1993) and Hirt and Sicilian (1985). The Navier-Stokes equations are as follows (Flow Science, 2012):

1. Mass Continuity Equation

The general mass continuity equation is:

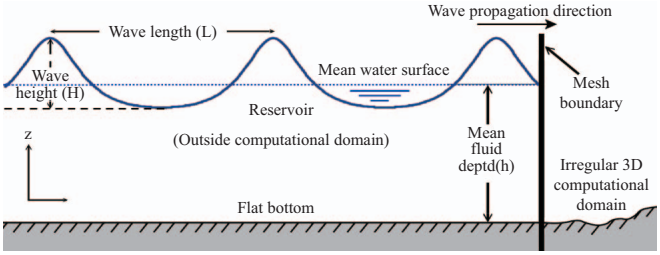

Fig. 3. Stokes wave entering the left side of a computational domain from a reservoir with a flat bottom.

$$V_F \frac{\partial \rho}{\partial t} + \frac{\partial}{\partial x}\left(\rho u A_x\right) + \frac{\partial}{\partial y}\left(\rho v A_y\right) + \frac{\partial}{\partial z}\left(\rho w A_z\right) = R_{DIF}$$

where V_F is the fractional volume open to flow, ρ is the fluid density, and R_{DIF} is a turbulent diffusion term. The velocity components u, v, and w are in the coordinate directions x, y, and z respectively. The term A_x is the fractional area open to flow in the x-direction, and A_y and A_z are similar area fractions for flow in the y and z directions, respectively.

2. Momentum Equations

The momentum equations for the fluid velocity components (u, v, and w) in the three coordinate directions are the Navier-Stokes equations with additional terms.

$$\frac{\partial u}{\partial t} + \frac{1}{V_F}\left\{uA_x\frac{\partial u}{\partial x} + vA_y\frac{\partial u}{\partial y} + wA_z\frac{\partial u}{\partial z}\right\} = -\frac{1}{\rho}\frac{\partial P}{\partial x} + f_x - \frac{R_{SOR}}{\rho V_F}(u - \delta u_s)$$

$$\frac{\partial v}{\partial t} + \frac{1}{V_F}\left\{uA_x\frac{\partial v}{\partial x} + vA_y\frac{\partial v}{\partial y} + wA_z\frac{\partial v}{\partial z}\right\} = -\frac{1}{\rho}\frac{\partial P}{\partial y} + f_y - \frac{R_{SOR}}{\rho V_F}(v - \delta v_s)$$

$$\frac{\partial w}{\partial t} + \frac{1}{V_F}\left\{uA_x\frac{\partial w}{\partial x} + vA_y\frac{\partial w}{\partial y} + wA_z\frac{\partial w}{\partial z}\right\} = -\frac{1}{\rho}\frac{\partial P}{\partial z} + f_z - \frac{R_{SOR}}{\rho V_F}(w - \delta w_s)$$

In these equations, (f_x, f_y, and f_z) are viscous accelerations, R_{SOR} is a mass source, and the final terms account for the injection of mass at a source represented by a geometrical component.

3. Stokes Wave Generator

The model is based on the fifth-order Stokes wave theory developed by Fenton (1985).

As shown in Fig. 3, wave trains are assumed to originate in flat bottom reservoirs in computational domains and proceed through mesh boundaries. The reference system (x, z) is established with its origin fixed at the bottom, $+x$ moving in the wave propagation direction, and $+z$ moving upward. The wave is characterized by the wave height H, wave length L, and wave period T. The undisturbed water depth is h = constant. Water elevation η is time-dependent and measured along $+z$ from the bottom to the water surface.

4. Free Surface Boundary

The free surface in this hydrodynamic model is captured using the volume of fluid (VOF) method (Hirt and Nichols, 1981). The VOF method is expressed (Flow Science, 2012)

$$\frac{\partial F}{\partial t}+\frac{1}{V_F}\left[\frac{\partial}{\partial x}\left(FA_x u\right)+\frac{\partial}{\partial y}\left(FA_y v\right)+\frac{\partial}{\partial z}\left(FA_z w\right)\right]=F_{DIF}$$

where V_F is the diffusion coefficient, and F_{DIF} is the turbulent diffusion.

5. Turbulence Closure Model

The turbulence was modeled using a RNG modified version of the k-ε turbulence closure model. The scour potential model is applicable to all turbulent models. However, the RNG model is generally recommended for simulating bottom boundaries featuring drastic transformations.

6. Scour Potential Model

The scour potential model computes excess shear stress beyond which scouring may occur along solid surfaces. Using the scour potential model enables researchers to evaluate the likelihood of scouring without the complexity and expense of using a full scour model. The scour potential model only requires the definition of critical shear stress above which scouring is expected. When the critical shear stress is set as zero, the model outputs the magnitude of the actual shear stress.

V. NUMERICAL SIMULATION OF TIDAL CURRENT FIELD IN THE SEA AREA NEAR THE BREAKWATER

The numerical simulation process in this study was divided into the preprocessing, numerical computation, and postprocessing stages. Preprocessing stage: The appropriate control module was selected, the initial and boundary conditions were determined, the computational grid was established, and the computational nodes were generated. Numerical computational stage: The discrete equation was imported, the computational control parameters were set, and the discrete equation was computed. If the computation was not converged, then the control parameters were adjusted before the discrete equation was imported. If the computation was converged, then the result was displayed and exported using postprocessing.

1. Computation Domain and Boundary Conditions

Tidal current field computational domain: First, grid independence and computational domain reasonableness testing were completed. The x- and y-direction grids were set as (δx) = (δy) = 50 m. The grid in the vertical water layer was set as (δz) = 1 m. Second, the computational domain and boundary conditions were set. The Mailiao Harbor breakwater head was assumed to be the origin point, each tidal level boundary in the open sea of the computational domain was set as 8000 m north, south, and west of the breakwater head, and the harbor physical model was used as the requirement for the closing boundary (wall boundary). Specifically, the north-south length was 16 km, and the east-west width was 12 km. The bottom boundary was constructed according to multibeam sounding data. Active tidal level: The tidal level of the aforesaid open water boundary was calculated according to the harmonic tidal constants on the basis of the tidal record of an ADCP "W" in the Mailiao Harbor sea area from 14:00 May 3 to 19:00 May 9, 2012.

2. Tidal Current Field Simulation Results and Analysis

The simulation of flux and reflux conditions in the sea area near Mailiao Harbor experienced 12 floods and 12 ebbs. The flow-field conditions of various tidal intervals are discussed as follows.

1) Mailiao Harbor Flood Stage

The main tidal current directions tended to be identical in the flood stage, as shown in Fig. 4. In the flood stage at 22:30 on May 8, the south side of the breakwater was north-oriented, the north side of the breakwater turned east because of the topographic effect, and the tidal current velocity at both the northern and southern boundaries of the sea area was high, between 0.5 m/s and 1.0 m/s. The tidal current velocity in the northwest sea area was lower than 0.2 m/s. According to the relationship between the development scales of the high velocity zone and the tidal levels, a lower initial tide level of a flood stage indicates a larger developmental range of the high current velocity.

2) Mailiao Harbor High Tide Stage

In the high tide stage at 01:10 on May 9, as shown in Fig. 5. The head difference was reduced at high tide to form a slack tide, the tidal current velocity in the simulated area decreased rapidly, and the tidal current condition tended to ebb. For example, in the northwest and southwest sea areas far from the W station, the tidal current began to flow into open water.

3) Mailiao Harbor Ebb Tide Stage

In the ebb tide stage at 04:00 on May 9, as shown in Fig. 6. The boundary water-level fluctuation time sequence entered the ebb stage, the overall tidal current direction turned from north to south, and the high tidal current velocity region moved from the northern boundary to the southern boundary and nearly stabilized in the west to west-northwest sea area outside Mailiao Harbor. Near the western breakwater side, a southward extended band directed the high tidal current velocity system away from the origin of the breakwater head, the tidal current direction was between the south and the south-southeast, and the tidal current velocity was approximately 1.0 m/s.

4) Mailiao Harbor Low Tide Stage

In the low tide stage at 06:40 on May 9, as shown in Fig. 7. The whole water head was reduced to form slack water. At this point in time, the tidal current direction reversed toward the coastal area.

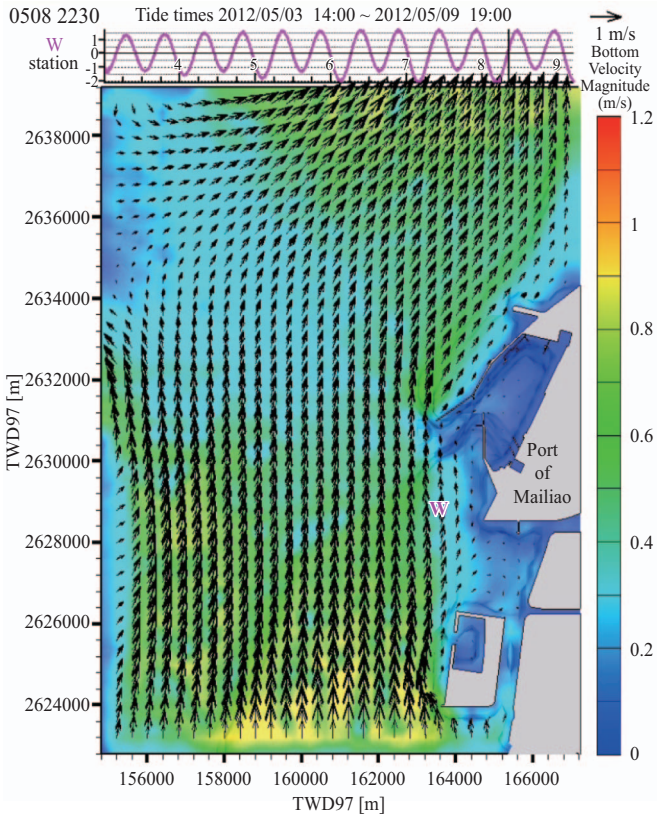

Fig. 4. Mailiao Harbor flood stage.

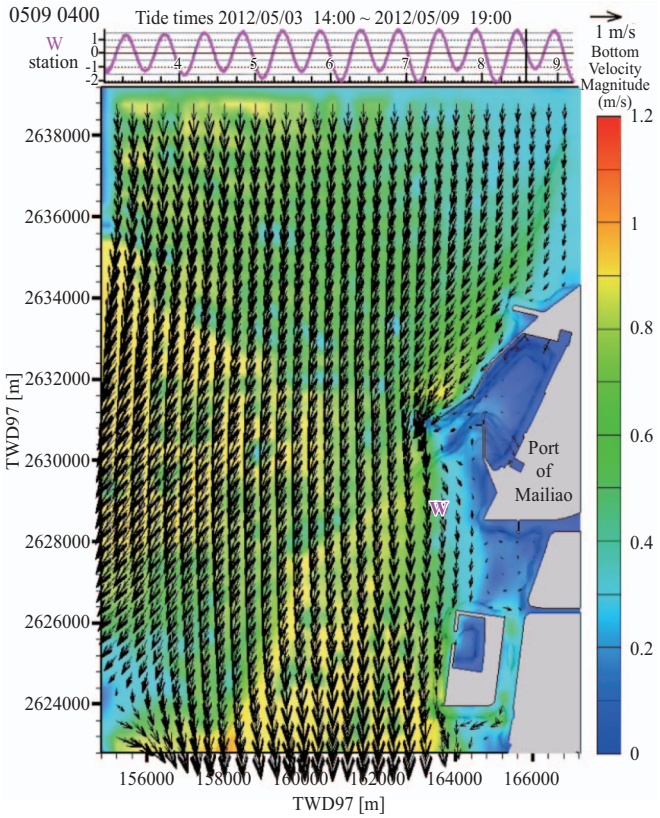

Fig. 6. Mailiao Harbor ebb tide stage.

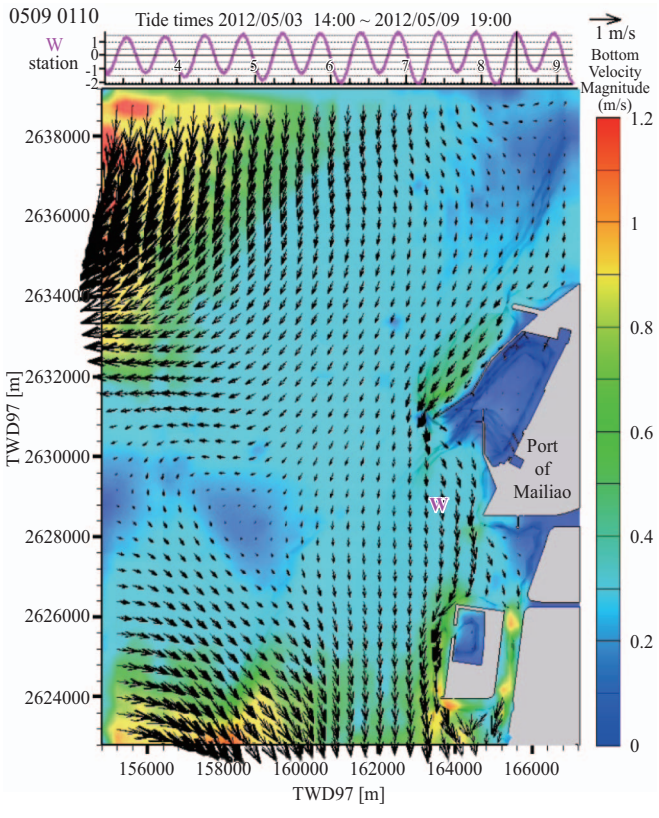

Fig. 5. Mailiao Harbor high tide stage.

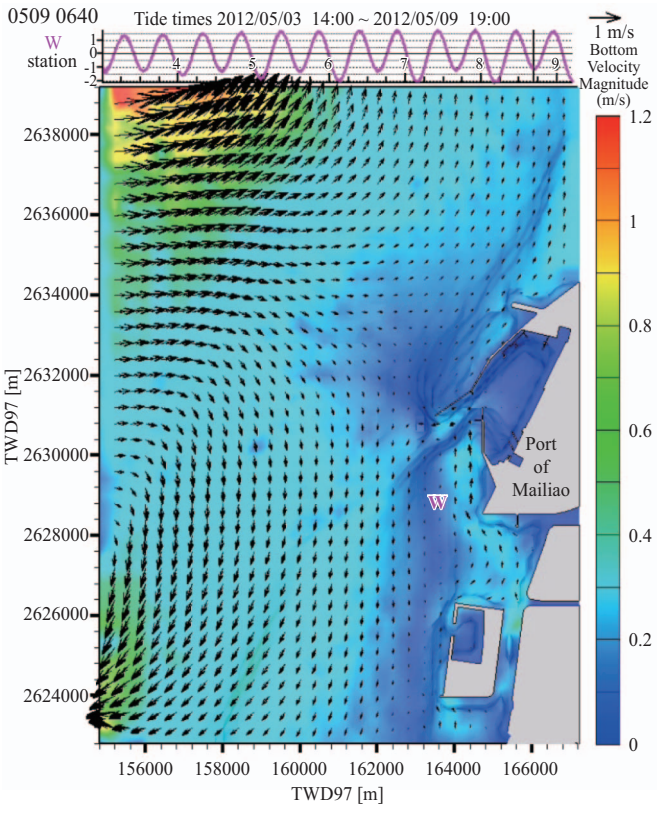

Fig. 7. Mailiao Harbor low tide stage.

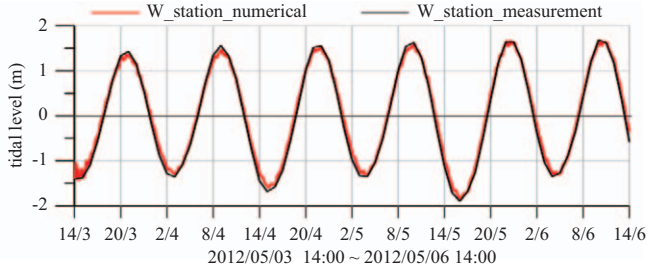

Fig. 8. Verification of tidal level by W station.

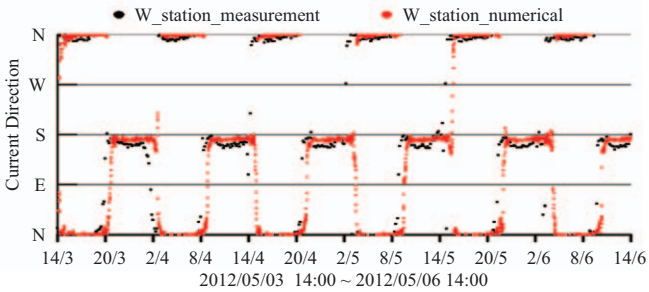

Fig. 9. Verification of tidal current direction by W station.

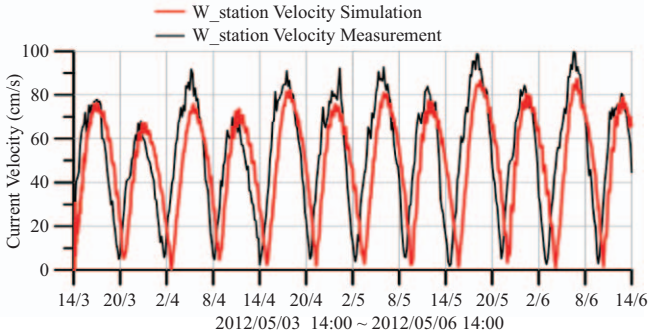

Fig. 10. Verification of tidal current velocity by W station.

5) Verification of Tidal Level, Tidal Current Direction, and Tidal Velocity

The coordinates of the W station were 23°45'38"N, 120°09'08"E, and the water depth was approximately 10 m. An ADCP was used to observe the tidal current direction, velocity, and tidal level at the sea surface and sea bed. The monitoring position is shown in Fig. 4. The observation period was 22 days, from May 3 to May 24, 2012. The verification result revealed that the numerical model matched the tidal level, current direction, and velocity observed by the ADCP "W", as shown in Figs. 8-10.

VI. NUMERICAL SIMULATION OF WAVE FIELD IN SEA AREA NEAR BREAKWATER

1. Computation Domain and Boundary Conditions

The computational domain was the sea area near the western breakwater head and eastern breakwater in Mailiao Harbor

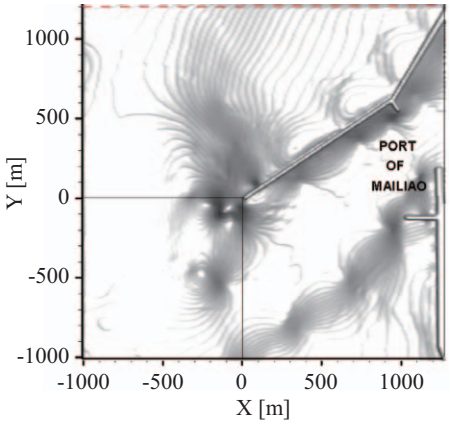

Fig. 11. Computational domain near the western breakwater head.

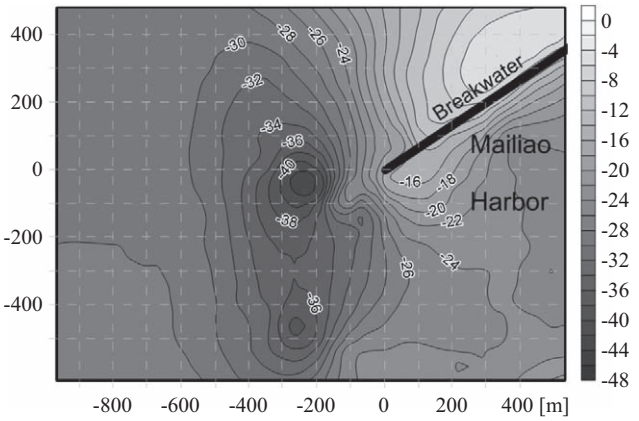

Fig. 12. Seafloor topography in Mailiao Harbor (in situ measurement in this study, 2011).

(2.3 × 2.2 km), the bottom boundary was determined according to the measured topographical data in the near sea area, as shown in Fig. 11. The related position of the scour area, as shown in Fig. 12.

According to the grid independence test results, the grid in the normal incidence direction (δy) was set as a 1/20 wavelength, the grid in the parallel incident wave direction (δx) was set as a 1/10 wavelength, and the vertical water layer grid (δz) was set as a 1/10 wave height. The total simulation time was set as 30 wave generation cycles, which occur when a fully developed wave completely passes through the observation zone. The northern boundary was an incident wave, and according to the typhoon wave estimation conditions of a 50-year return period in the open sea of Mailiao Harbor, the designed wave height was 5.9 m, and the wave period was 10.2 s.

2. Variations in Free Surface and Wave-Induced Current Velocity in Wave Field

Examining the free surface change in the numerical simulation is the most effective method of reviewing the rationality of the study results. For brevity, this study only used the simulation result of the 15th wave generation cycle to determine the flow velocity and free surface changes, as shown in

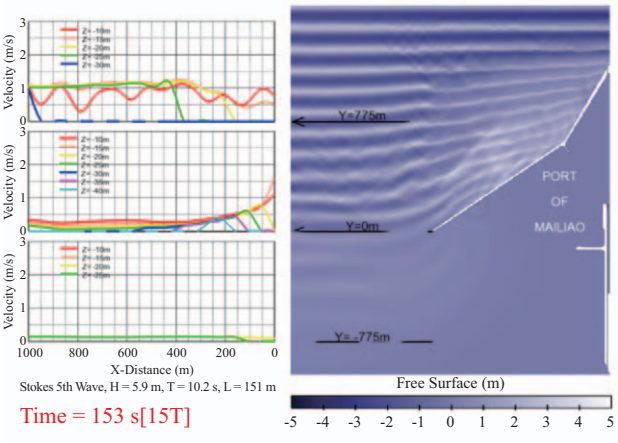

Fig. 13. Variations in free surface and wave-induced current speed in z-direction of 15 periods after waves were generated.

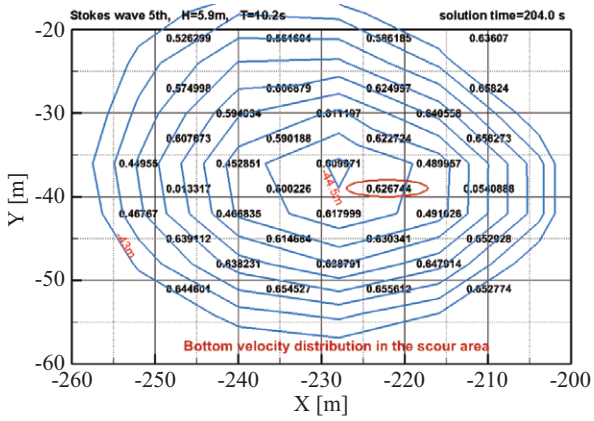

Fig. 14. Distribution of bottom flow velocity of 20 periods after waves were generated in scour area.

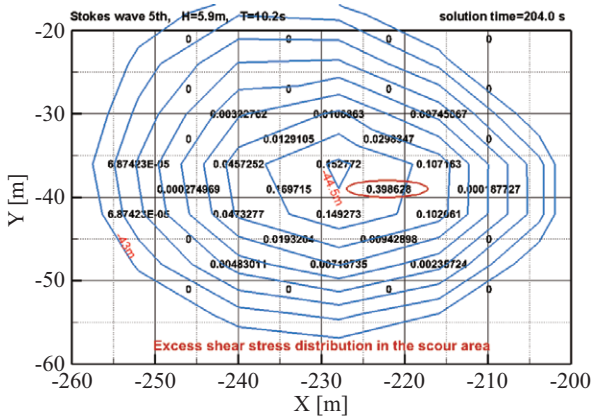

Fig. 15. Distribution of excess shear stress of 20 periods after waves were generated in scour area.

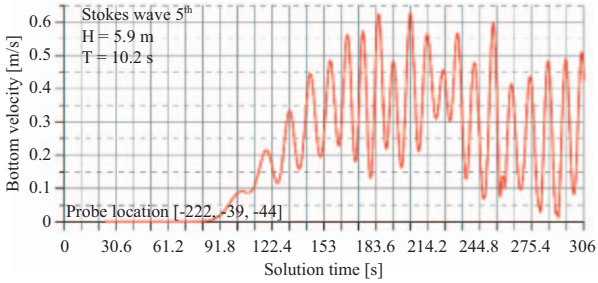

Fig. 16. Bottom flow velocity in time serial for coordinates [−222, −39, −44].

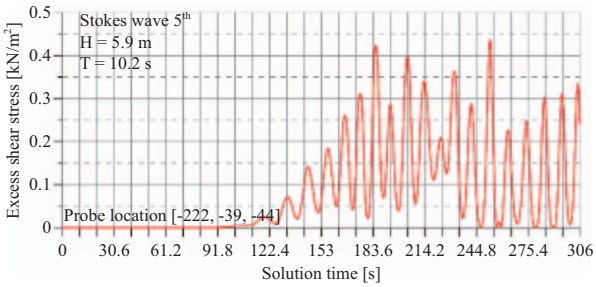

Fig. 17. Excess shear stress in time serial for coordinates [−222, −39, −44].

Fig. 13. Where the wave velocity magnitude ($\sqrt{u^2+v^2+w^2}$) profiles, Y = 775, 0, and −775 m, vertical stratification spacing was 5 m and extended 1000 m to the open water from the origin of the breakwater head. The velocity amplitude in the northern short-crested wave field stratification of breakwater was larger, the velocity amplitude in the downstream boundary wave field stratification was consistent, the velocity amplitude in wave stratification near the western side of the breakwater head was arranged normally , and a scour area occurred at 200 m. The profile of the 21st wave generation cycle flow condition of the incident wave in the northern sea area of Mailiao Harbor passing the western breakwater head is shown in the Appendix. The wave and breakwater head engaged in a violent coupling motion, the water particles fluctuated, the velocity increased to 4 m/s, and the flow field initiated by this wave condition influenced the near sea bed. The down-stream face of the breakwater head was shielded by the structure , and the vertical flow field remained at approximately 1 m/s while flowing upward.

3. Distribution of Bottom Flow Velocity and Excess Shear Stress in Scour Area

The scour trend of a moving bed can be rapidly estimated in the bottom boundary condition of a fixed bed according to excess shear stress (ESS = $\tau/\tau_{critical}$, $\tau = \rho u^2$). The distribution of wave-induced flow velocity and excess shear stress of the bottom in the scour area in the 20th wave generation cycle of the northward incident wave in Mailiao Harbor is shown in Figs. 14 and 15. The magnitude of flow velocity and excess shear stress varied with the wave generation cycle. The breakwater head still-water-level tangent point was the origin, and the red frame coordinates [x = –222 m, y = –39 m, and z = –44 m] were used for time series analysis, as shown in Figs. 16 and 17; the bottom flow velocity and excess shear stress time sequence exhibited consistent developmental trends.

4. Distribution of Vorticity Field in Scour Area

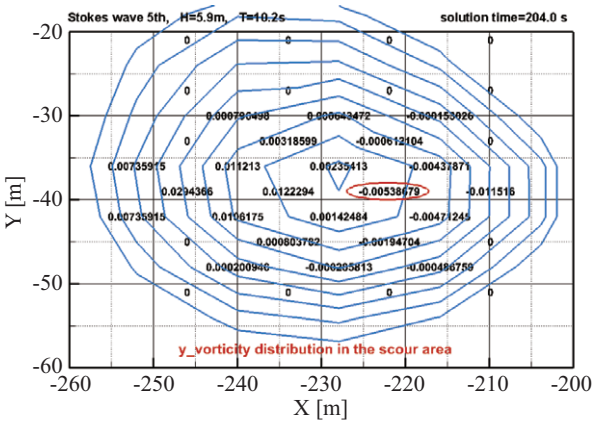

Fig. 18. Distribution of vorticity in y-direction in scour area.

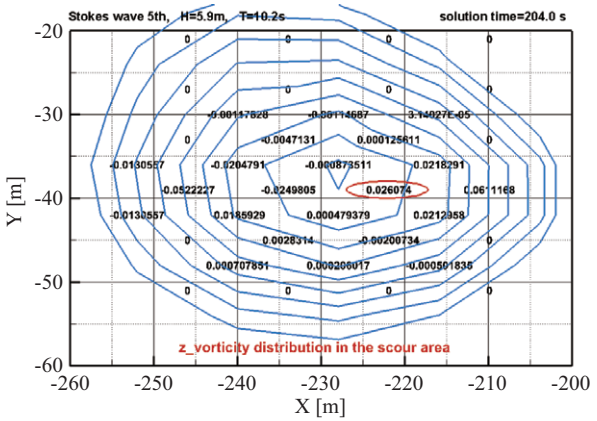

Fig. 19. Distribution of vorticity in z-direction in scour area.

The vortex developed and dissipated at the bottom of the scour area , where the strength scale of the vortex can be further analyzed according to the distribution and variation of the vorticity field in the scour area. The turbulent field can be expanded by the stretching and tilt of vorticity. The distribution of vorticity in the y and z directions of the bottom of the scour area in the 20th wave generation cycle of the northward incident wave in Mailiao Harbor is shown in Figs. 18 and 19, respectively. The y-direction vorticity was in a clockwise horizontal distribution, whereas the z-direction vorticity was in an anticlockwise vertical distribution. Figs. 20 and 21 show that vorticity occurred only at the bottom of the scour area or above the bottom of the scour area (–44 m).

VII. CONCLUSION

This hydrodynamic model was used for numerical simulation of the breakwater sea area in Mailiao Harbor. The computational domain was 12 × 16 km, the bottom boundary was used to measure geography, the boundary tidal level was used to simulate the tidal current field in the area, and the typhoon wave in the artificial conditions was used to simulate the wave field in the northern incident wave direction. The characteristics of the model were verified, and the results of the numerical model were similar to those regarding the tidal level, tidal current direction, and tidal velocity observed by the W station. The extreme typhoon wave conditions, including a wave height of 5.9 m and period of 10.2 s, were analyzed. Moreover, the flow-field change initiated by the wave field operation of 306 s (30 wave generation cycles) and wave was calculated. From its origin in the western breakwater head, the wave entered the model boundary from the north. The wave was obstructed by the northern side of the western breakwater and therefore formed a reflected wave. Thus, the wave height in this sea area and velocity magnitude in the wave field increased greatly. The sea area on the southern side of the western breakwater was shielded by the breakwater, and the wave height and velocity magnitude changes were smaller on the southern side of the western breakwater than they were on the northern side of the western breakwater. A positive correlation was observed between bottom flow velocity and excess shear stress over the scour area, and this relationship was also reflected in the scouring potential along the fixed bed. The fluid dynamic state in the area near the breakwater head was preliminarily determined by simulating the tidal current, wave field, and flow field, which were initiated by the wave. The wave current intersection and drift-sand moving bed can be further tested to clarify the mechanisms and variations of breakwater head erosion.

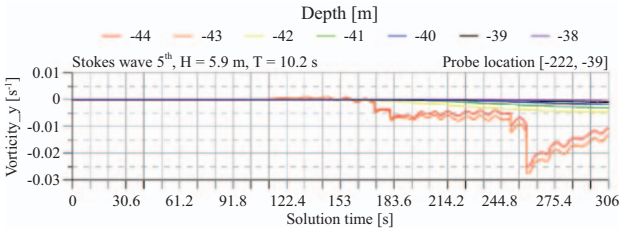

Fig. 20. Y-direction vorticity for coordinates [−222, −39] in multiple layers.

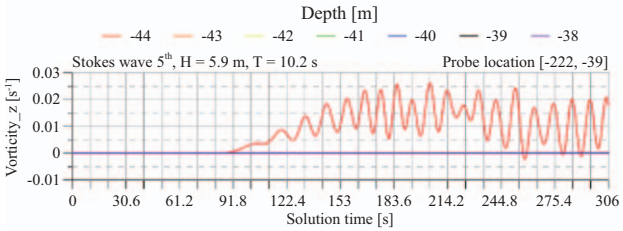

Fig. 21. Z-direction vorticity probe for coordinates [−222, −39] in multiple layers.

ACKNOWLEDGMENTS

This study was supported by the Harbor and Marine Technology Center, Institute of Transportation, Ministry of Transportation and Communications, R.O.C., Project No. MOTC-IOT-103-H2DB005d.

APPENDIX

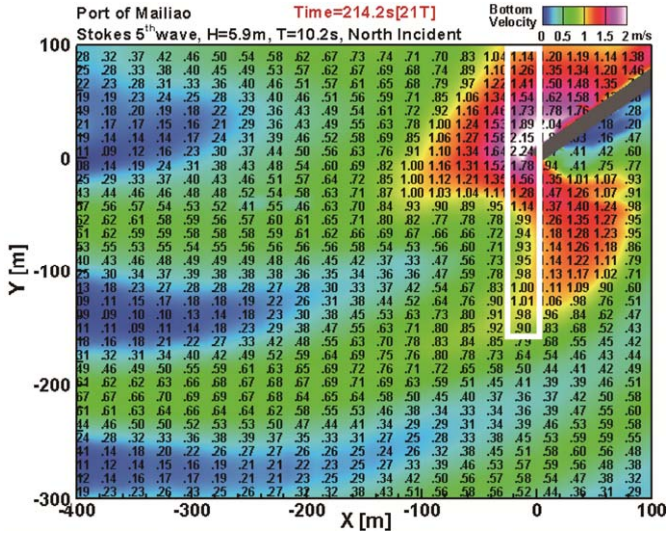

Bottom flow velocity of 21 periods after waves were generated.

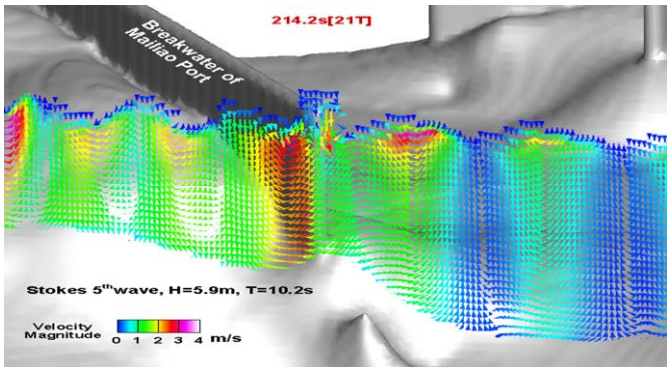

Velocity profile frame (white rectangular border in the previous fig.) of the flow condition of 21 periods after waves were generated.

REFERENCES

ACHARYA, A. (2011). Experimental study and numerical simulation of flow and sediment transport around a series of spur dikes. Ph.D. thesis, Univ. of Arizona, USA.

Dentale, F., G. Donnarumma and E. Pugliese Carratelli (2012). Wave Run Up and Reflection on Tridimensional Virtual Breakwater. Journal of Hydrogeology & Hydrologic Engineering, 1:1.

Gokce, T., B. M. Sumer and J. Fredsøe (1994). Scour around the head of a vertical wall breakwater. Proc. International Conference on Hydro-Technical Engineering for Port and Harbor Construction, Hydro-Port' 94, Yokosuka, Japan 2, 1097-1116.

Hirt, C. W. and B. D. Nichols (1981). Volume of fluid (vof) method for the dynamics of free boundaries. Journal of Computational Physics 39(1), 201-225.

Hirt, C. W. and J. M. Sicilian (1985). A porosity technique for the definition obstacles in rectangular cell meshes. Proceedings of the Fourth International Conference on Numerical Ship Hydrodynamics, National Academy of Sciences, 1985, Washington D.C., USA, 450-568.

Hirt, C. W. (1993). Volume-fraction techniques: powerful tools for wind engineering. Journal of Wind Engineering and Industrial Aerodynamics 46-47, 327-338.

Lai, J. W. (2009). Experimental and numerical studies on wave propagation over coarse grained sloping beach. Ph.D. thesis, National Cheng Kung University, Taiwan, Republic of China.

Myrhaug, D., H. Rue and A. Tørum (2004). Tentative engineering approach to scour around breakwaters in random waves. Coastal Engineering 51, 1051-1065.

Myrhaug, D. and M. C. Ong (2009). Random wave-induced scour at the trunk section of a breakwater. Coastal Engineering 56, 688-692.

Sato, S. and I. Irie (1970). Variation of topography of sea-bed caused by the construction of breakwaters. Proc. 12th Int. Conf. Coastal Eng., Washington D.C., USA, ASCE 2, 1301-1319.

Sumer, B. M. and J. Fredsøe (1997). Scour at the head of a vertical-wall breakwater. Coastal Engineering 29, 201-230.

Sumer, B. M. and J. Fredsøe (2000). Experimental study of 2D scour and its protection at a rubble-mound breakwater. Coastal Engineering 40, 59-87.

Sumer, B. M., Richard J. S. Whitehouse and A. Tørum (2001). Scour around coastal structures: A summary of recent research. Coastal Engineering 44(2), 153-190.

Sumer, B. M., J. Fredsøe, A. Lamberti, B. Zanuttigh, M. Dixen, K. Gislason and A. F. Di Penta (2005). Local scour at roundhead and along the trunk of low crested structures. Coastal Engineering 52, 995-1025.